SCIENTIFIC REPⓄRTS

OPEN

Analyzing the Quantum Zeno and anti-Zeno effects using optimal projective measurements

Muhammad Junaid Aftab & Adam Zaman Chaudhry

Measurements in quantum mechanics can not only effectively freeze the quantum system (the quantum Zeno effect) but also accelerate the time evolution of the system (the quantum anti-Zeno effect). In studies of these effects, a quantum state is prepared repeatedly by projecting the quantum state onto the initial state. In this paper, we repeatedly prepare the initial quantum state in a different manner. Instead of only performing projective measurements, we allow unitary operations to be performed, on a very short time-scale, after each measurement. We can then repeatedly prepare the initial state by performing some projective measurement and then, after each measurement, we perform a suitable unitary operation to end up with the same initial state as before. Our objective is to find the projective measurements that minimize the effective decay rate of the quantum state. We find such optimal measurements and the corresponding decay rates for a variety of system-environment models such as the pure dephasing model and the spin-boson model. We find that there can be considerable differences between this optimized effective decay rate and the usual decay rate obtained by repeatedly projecting onto the initial state. In particular, the Zeno and anti-Zeno regimes can be considerably modified.

Rapid repeated measurements can slow down the time evolution of a quantum system, an effect known as the Quantum Zeno effect (QZE)[1]. It has also been found that if the measurements are not rapid enough, an opposite effect, known as the Quantum anti-Zeno effect (QAZE), can occur - the measurements can actually accelerate quantum transitions[2,3]. Both the QZE and the QAZE have attracted widespread interest both theoretically and experimentally due to their relevance to the foundations of quantum mechanics as well as possible applications in quantum technologies[4–41]. Generally, the analysis of QZE and QAZE for open quantum systems assumes that one continues to repeatedly prepare the initial state of the quantum system by repeatedly projecting the system onto the initial state. However, one can prepare the initial state of the system repeatedly in a different way. Instead of restricting ourselves to performing the same projective measurement again and again, we can instead think of allowing ourselves to perform a unitary operation after each projective measurement. This means that we are no longer restricted to performing the same projective measurement to repeatedly prepare the initial state. We can then use this freedom in the choice of the projective measurement to think about maximizing the survival probability of the system quantum state. Our goal is to find the projective measurements that maximize this survival probability, or, equivalently, minimize the effective decay rate. Thus we arrive at a strategy that allows us to maximally protect the quantum state. We can then study the quantum Zeno and anti-Zeno effects with such optimal projective measurements.

We start off by considering a single two-level system coupled to an arbitrary environment. Starting from an arbitrary initial state, our goal is to find the projective measurements followed by appropriate unitary operators that can be used to repeatedly prepare the initial state such that the survival probability of the quantum state is maximized. We find a general condition that allows us to do so. Namely, we find that the dynamically evolving Bloch vector of the quantum system determines the optimal projective measurement and, in turn, the optimal survival probability. Furthermore, the optimal projective measurements depend on the time interval between the measurements. This contrasts sharply with the usual scenario where the same projective measurement is performed repeatedly, regardless of the measurement interval. Applications of the condition derived are illustrated by studying the usual decay rate and the optimized decay rate for the population decay model, the pure dephasing model, and the spin-boson model. Since the behaviour of the effective decay rate allows us to identify

School of Science & Engineering, Lahore University of Management Sciences (LUMS), Opposite Sector U, D.H.A, Lahore, 54792, Pakistan. Correspondence and requests for materials should be addressed to A.Z.C. (email: adam.zaman@lums.edu.pk).

the Quantum Zeno and anti-Zeno regimes, we can instead use this optimized decay rate to look at the Quantum Zeno and anti-Zeno effects. We then consider a collection of two-level systems interacting with a common environment. In this case, finding the optimal projective measurement is a very difficult problem. However, we can restrict ourselves to measurements that project onto spin coherent states since these are the measurements that can be performed relatively easily experimentally. For this scenario, we again derive the optimal measurements and the optimized decay rate for the pure dephasing case as well as the more general scenario with both dephasing and relaxation present. Once again, we find that there can be signficant differences between the unoptimized decay rate and the optimized decay rate. These differences translate to differences in the QZE and the QAZE.

Results

Optimal projective measurements for a single two-level system.   Let us begin by considering a single two-level system interacting with an arbitrary environment. The Hamiltonian of the system is H_S, the environment Hamiltonian is H_B, and there is some interaction between the system and the environment that is described by the Hamiltonian V. The total system-environment Hamiltonian is thus $H = H_S + H_B + V$. At time $t = 0$, we prepare the system state $|\psi\rangle$. In the usual treatment of the quantum Zeno and anti-Zeno effects, repeated projective measurements described by the projector $|\psi\rangle\langle\psi|$ are then performed on the system with time interval τ. The survival probability of the system state after one measurement is then $s(\tau) = \mathrm{Tr}_{S,B}[(|\psi\rangle\langle\psi| \otimes \mathbb{1})e^{iH_S\tau}e^{-iH\tau}\rho(0)e^{iH\tau}e^{-iH_S\tau}]$, where $\mathrm{Tr}_{S,B}$ denotes taking the trace over the system and the environment, $\rho(0)$ is the initial combined state of the system and the environment, and the evolution of the system state due to the system Hamiltonian itself has been eliminated via a suitable unitary operation just before performing the measurement[28,38,42]. Assuming that the system-environment correlations can be neglected, the survival probability after N measurements can be written as $[s(\tau)]^N = e^{-\Gamma(\tau)N\tau}$, thereby defining the effective decay rate $\Gamma(\tau)$. It should be noted that the behaviour of the effective decay rate $\Gamma(\tau)$ as a function of the measurement interval allows us to identify the Zeno and anti-Zeno regimes. Namely, if $\Gamma(\tau)$ increases as τ increases, we are in the Zeno regime, while if $\Gamma(\tau)$ decreases if τ increases, we are in the anti-Zeno regime[2,9,18,28,38].

We now consider an alternative way of repeatedly preparing the initial state with time interval τ. Once again, we start from the initial system state $|\psi\rangle$. After time τ, we know that the state of the system is given by the density matrix $\rho_S(\tau) = \mathrm{Tr}_B[e^{iH_S\tau}e^{-iH\tau}\rho(0)e^{iH\tau}e^{-iH_S\tau}]$, where once again the evolution due to the free system Hamiltonian has been removed. Now, instead of performing the projective measurement $|\psi\rangle\langle\psi|$, we perform an arbitrary projective measurement given by the projector $|\chi\rangle\langle\chi|$. The survival probability is then $s(\tau) = \mathrm{Tr}_S[(|\chi\rangle\langle\chi|)\rho_S(\tau)]$, and the post-measurement state is $|\chi\rangle$. By performing a unitary operation U_R on the system state on a short timescale such that $U_R|\chi\rangle = |\psi\rangle$, we can again end up with the initial state $|\psi\rangle$ after the measurement. This process can then, as before, repeated again and again to repeatedly prepare the system state $|\psi\rangle$. Once again, if the correlations between the system and the environment can be neglected, we can write the effective decay rate as $\Gamma(\tau) = -\frac{1}{\tau}\ln s(\tau)$. But now, we can, in principle, via a suitable choice of the projector $|\chi\rangle\langle\chi|$, obtain a larger survival probability (and a correspondingly smaller decay rate) than what was obtained with repeatedly using projective measurements given by the projector $|\psi\rangle\langle\psi|$. The question, then, is what is this projector $|\chi\rangle\langle\chi|$ that should be chosen to maximize the survival probability?

For an arbitrary quantum system, it is difficult to give a general condition or formalism that will predict this optimal projective measurement. However, most studies of the effect of repeated quantum measurements on quantum systems have been performed by considering the quantum system to be a single two-level system[3]. Let us now show that if the quantum system is a two-level system, then it is straightforward to derive a general method for calculating the optimal projective measurements that need to be performed as well as an expression for the optimized decay rate. We start from the observation that the system density matrix at time τ, just before the measurement, can be written as

$$\rho_S(\tau) = \frac{1}{2}(1 + n_x(\tau)\sigma_x + n_y(\tau)\sigma_y + n_z(\tau)\sigma_z) = \frac{1}{2}(1 + \mathbf{n}(\tau) \cdot \boldsymbol{\sigma}), \tag{1}$$

where $\mathbf{n}(\tau)$ is the Bloch vector of the system state. We are interested in maximizing the survival probability $s(\tau) = \mathrm{Tr}_S[(|\chi\rangle\langle\chi|)\rho_S(\tau)]$. It is clear that we can also write

$$|\chi\rangle\langle\chi| = \frac{1}{2}(1 + n_x'\sigma_x + n_y'\sigma_y + n_z'\sigma_z) = \frac{1}{2}(1 + \mathbf{n}' \cdot \boldsymbol{\sigma}), \tag{2}$$

where $\mathbf{n}'$ is a unit vector corresponding to the Bloch vector for the projector $|\chi\rangle\langle\chi|$. Using Eqs (1) and (2), we find that the survival probability is

$$s(\tau) = \frac{1}{2}(1 + \mathbf{n}(\tau) \cdot \mathbf{n}'). \tag{3}$$

It should then be obvious how to find the optimal projective measurement $|\chi\rangle\langle\chi|$ that needs to be performed. The maximum survival probability is obtained if $\mathbf{n}'$ is parallel to $\mathbf{n}(\tau)$. If we know $\rho_S(\tau)$, we can find out $\mathbf{n}(\tau)$. Consequently, $\mathbf{n}'$ is simply the unit vector parallel to $\mathbf{n}(\tau)$. Once we know $\mathbf{n}'$, we know the projective measurement $|\chi\rangle\langle\chi|$ that needs to be performed. The corresponding optimal survival probability is given by

$$s^*(\tau) = \frac{1}{2}(1 + \|\mathbf{n}(\tau)\|), \tag{4}$$

where $\|\mathbf{n}(\tau)\|$ is the magnitude of the vector $\mathbf{n}(\tau)$. Now, if we ignore the correlations between the system and environment, which is valid for weak system-environment coupling, we derive the effective decay rate of the quantum state with optimal projective measurements to be $\Gamma(\tau) = -\frac{1}{\tau}\ln s^*(\tau)$. Before moving on to investigate this optimal effective decay rate for a variety of system-environment models and comparing it with the usual effective decay rate, let us note that at short measurement intervals, the two effective decay rates are expected to be very similar since the system state has barely evolved. Eqs (3) and (4), with $\mathbf{n}(\tau)$ being very close to the Bloch vector of the initial state, support this assertion.

The population decay model. To begin, we consider the paradigmatic population decay model. The system-environment Hamiltonian is (we use $\hbar = 1$ throughout)

$$H = \frac{\varepsilon}{2}\sigma_z + \sum_k \omega_k b_k^\dagger b_k + \sum_k (g_k^* b_k \sigma^+ + g_k b_k^\dagger \sigma^-), \tag{5}$$

where ε is the energy difference between the two levels, σ_z is the standard Pauli matrix, σ^+ and σ^- are the raising and lowering operators, and b_k and $b_k^\dagger$ are the annihilation and creation operators for mode k of the environment. It should be noted that we have made the rotating-wave approximation. This system-environment Hamiltonian is widely used to study, for instance, spontaneous emission[43]. We consider the very low temperature regime. We initially prepare the system-environment state $|\uparrow_z, 0\rangle$ that describes the two-level system to be in the excited state and the environment oscillators to be in their ground state. Ordinarily, in the studies of the QZE and the QAZE, the system is repeatedly projected onto the excited state with time interval τ. As discussed before, we, on the other hand, allow the system to be projected onto some other state such that the effective decay rate is minimized. To find this optimal projective measurement, we need to understand how the Bloch vector of the system evolves in time. Due to the structure of the system-environment Hamiltonian, the system-environment state at a later time τ can be written as $|\psi(t)\rangle = f(t)|\uparrow_z, 0\rangle + \sum_k f_k(t)|\downarrow_z, k\rangle$, where $|\downarrow_z, k\rangle$ means that the two-level system is in the ground state and that mode k of the environment has been excited. It then follows that the density matrix of the system at time τ is

$$\rho_S(\tau) = \begin{bmatrix} |f(t)|^2 & 0 \\ 0 & \sum_k |f_k(t)|^2 \end{bmatrix} \tag{6}$$

We consequently find that the components of the Bloch vector of the system are $n_x(t) = n_y(t) = 0$, while $n_z(t) = 1 - 2\sum_k |f_k(t)|^2$. Thus, we have a nice interpretation for the dynamics of the system. Initially, the system is in the excited state. As time goes on, the coherences remain zero, and the probability that the system makes a transition to the ground state increases. In other words, initially the Bloch vector of the system is a unit vector with $n_z(0) = 1$. The Bloch vector then decreases in magnitude (while keeping the x and y components zero) until the size of the Bloch vector becomes zero. The Bloch vector thereafter flips direction and increases in length until effectively $n_z(t) = -1$. Since the direction of the Bloch vector corresponding to the optimal measurement is parallel to the Bloch vector of the system, we find that if the measurement interval is short enough such that $n_z(\tau) > 0$, then we should keep on applying the projector $|\uparrow_z\rangle\langle\uparrow_z|$. On the other hand, if the measurement interval is large enough so that $n_z(\tau) < 0$, then we should rather apply the projector $|\downarrow_z\rangle\langle\downarrow_z|$, and then, just after the measurement, apply a π pulse so as to end up with the system state $|\uparrow_z\rangle$ again. In other words, the time $t = \tau^*$ at which the Bloch vector flips direction is of critical importance to us and needs to be found in order to optimize the effective decay rate. To find this time, we assume that the system and the environment are weakly coupled and thus we can use a standard master equation to analyze the dynamics of the system. Since we numerically solve this master equation, we might as well put back in the non-rotating wave approximation terms so that the system-environment interaction that we consider in solving the master equation is $\sum_k \sigma_x(g_k^* b_k + g_k b_k^\dagger)$. The master equation that we use can be written as[44]

$$\frac{d\rho_S(t)}{dt} = i[\rho_S(t), H_S] + \int_0^t ds\{[\overline{F}(t, s)\rho_S(t), F]C_{ts} + \text{h.c.}\}, \tag{7}$$

where the system Hamiltonian is $H_S = \frac{\varepsilon}{2}\sigma_z$, the system-environment interaction Hamiltonian has been written as $F \otimes B$ with $F = \sigma_x$ and $B = \sum_k (g_k^* b_k + g_k b_k^\dagger)$, $\overline{F}(t, s) = e^{iH_S(t-s)}Fe^{-iH_S(t-s)}$, and h.c. denotes the hermitian conjugate. Here the environment correlation function C_{ts} is defined as $C_{ts} = \text{Tr}_B[\widetilde{B}(t)\widetilde{B}(s)\rho_B]$ where $\widetilde{B}(t) = e^{iH_B t}Be^{-iH_B t}$ and $\rho_B = e^{-\beta H_B}/Z_B$ with Z_B the partition function and β the inverse temperature. To find the environment correlation function, we introduce the spectral density function $J(\omega) = G\omega^s\omega_c^{1-s}e^{-\omega/\omega_c}$, where G parametrizes the system-environment coupling strength, s characterizes the Ohmicity of the environment, and ω_c is the cutoff frequency. We can then numerically solve this differential equation to find the system density matrix at any time t and consequently the Bloch vector of the system. We consequently know the optimal projective measurement that needs to performed.

We now present a computational example. We plot the single measurement survival probability [see Fig. 1(a)] and the effective decay rate [see Fig. 1(b)] as a function of the measurement interval τ. The dotted lines illustrate what happens if we keep on projecting the system state onto $|\uparrow_z\rangle$. For a small measurement interval, the optimal measurement is $|\uparrow_z\rangle\langle\uparrow_z|$ since the system Bloch vector has only a positive z-component. On the other hand, when the measurement interval is long enough such that between each measurement the Bloch vector flips direction, then to maximize the survival probability we should project onto the state $|\downarrow_z\rangle$ and then apply a π pulse. Doing so,
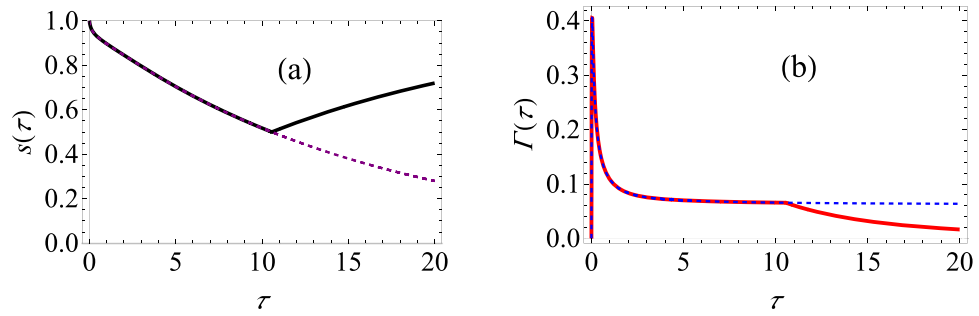
Figure 1. Behaviour of both the survival probability and the effective decay rate for the population decay model. (**a**) $s(\tau)$ versus τ. The purple dashed curve shows the survival probability if the excited state is repeatedly measured; the black curve shows the survival probability if the optimal projective measurement is repeatedly made. (**b**) $\Gamma(\tau)$ versus τ. The blue dashed curve shows the decay rate if the excited state is repeatedly measured; the solid red curve shows the decay rate if the optimal projective measurement is repeatedly made. We set $\varepsilon = 1$, and we have used $G = 0.01$ and $\omega_c = 50$. Throughout, we are using dimensionless units with $\hbar = 1$. In this case, $\tau^* \approx 10.6$.

we can obtain a higher survival probability or, equivalently, a lower effective decay rate. This is precisely what we observe from the figure. For this population decay case, we find that if the measurement interval is larger than $\tau^* \approx 10.6$, then we are better off by performing the measurement $|{\downarrow_z}\rangle\langle{\downarrow_z}|$. There is also a small change in the anti-Zeno behaviour. For our modified strategy of repeatedly preparing the quantum state, we find that beyond measurement interval $\tau = \tau^*$, there is a sharper signature of anti-Zeno behaviour as compared to the usual strategy of repeatedly measuring the excited state of the system.

Pure dephasing model. We now analyze our strategy for the case of the pure dephasing model[44]. The system-environment Hamiltonian is given by

$$H = \frac{\varepsilon}{2}\sigma_z + \sum_k \omega_k b_k^\dagger b_k + \sigma_z \sum_k (g_k^* b_k + g_k b_k^\dagger). \tag{8}$$

In contrast with the previous population decay model, the system-environment coupling term now contains σ_z instead of σ_x. This difference implies that the diagonal entries of the system density matrix $\rho_S(t)$ (in the $|{\uparrow_z}\rangle, |{\downarrow_z}\rangle$ basis) cannot change - only dephasing can possibly take place, which is the reason that this model is known as the pure dephasing model[28]. Furthermore, this pure dephasing model is exactly solvable. The off-diagonal elements of the density matrix undergo both unitary time evolution due to the system Hamiltonian and non-unitary time evolution due to the coupling with the environment. Assuming the initial state of the total system is the standard product state $\rho_S(0) \otimes \rho_B$, the off-diagonals of the density matrix $[\rho_S(t)]_{mn}$, once the evolution due to the system Hamiltonian itself is removed, are given by $[\rho_S(t)]_{mn} = [\rho_S(0)]_{mn} e^{-\gamma(\tau)}$ where $\gamma(t) = \sum_k 4|g_k|^2 \frac{(1 - \cos(\omega_k t))}{\omega_k^2} \coth\left(\frac{\beta\omega_k}{2}\right)$[28]. Note the absence of the energy gap ε - this is simply because the evolution due to the system Hamiltonian $\frac{\varepsilon}{2}\sigma_z$ has been removed. The removal of this evolution on a very short time-scale is justified since the time required for single-qubit operations experimentally (in the nanosecond and smaller regime[45,46]) can be much smaller than the measurement interval (in the microsecond regime[47]). Writing an arbitrary initial state of the system as $|\psi\rangle = \cos\left(\frac{\theta}{2}\right)|{\uparrow_z}\rangle + \sin\left(\frac{\theta}{2}\right)e^{i\phi}|{\downarrow_z}\rangle$, it is straightforward to find that

$$n_x(t) = e^{-\gamma(t)} n_x(0), \quad n_y(t) = e^{-\gamma(t)} n_y(0), \quad n_z(t) = n_z(0). \tag{9}$$

The optimal survival probability obtained using optimized measurements is then

$$s^*(\tau) = \frac{1}{2}\left(1 + \sqrt{n_z(0)^2 + (e^{-\gamma(\tau)})^2(n_x(0)^2 + n_z(0)^2)}\right), \tag{10}$$

where Eq. (4) has been used. On the other hand, if we keep on preparing the initial state $|\psi\rangle$ by using the projective measurements $|\psi\rangle\langle\psi|$, we find that

$$s(\tau) = \frac{1}{2}(1 + n_z(0)^2 + e^{-\gamma(\tau)}(n_x(0)^2 + n_z(0)^2)). \tag{11}$$

We now analyze Eqs (10) and (11) to find conditions under which we can lower the effective decay rate by using optimized projective measurements. It is clear that if the initial state, in the Bloch sphere picture, lies in the equatorial plane, then $n_z(0) = 0$ while $n_x(0)^2 + n_y(0)^2 = 1$. In this case, Eqs (10) and (11) give the same survival probability. Thus, in this case, there is no advantage of using our strategy of optimized measurements as compared with the usual strategy. Another way to see this is that, in the Bloch sphere picture, the magnitude of the time evolved Bloch vector of the density matrix reduces such that the time evolved Bloch vector is always parallel to the Bloch vector of the initial pure system state. As argued before, the optimal projector to measure at time τ, $|\chi\rangle\langle\chi|$, must
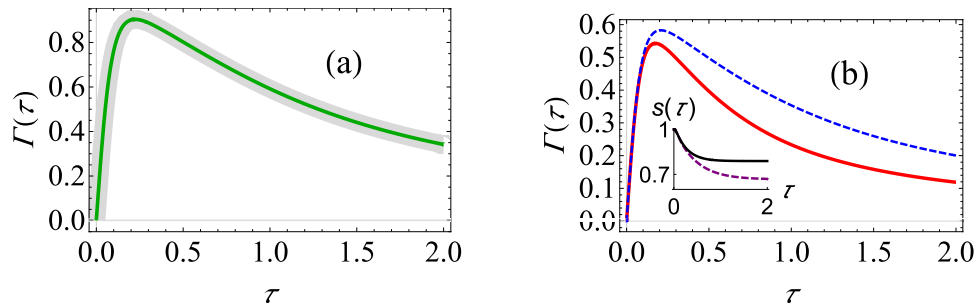
Figure 2. Graphs of the effective decay rate under making optimal projective measurements in the pure dephasing model. (**a**) $\Gamma(\tau)$ versus τ for the initial state specified by the Bloch vector $(1, 0, 0)$. The thickened light gray curve curve shows the decay rate if the initial state is repeatedly measured; the green curve shows the decay rate if the optimal projective measurement is repeatedly made. It is clear from the figure that the two curves identically overlap. We have used $G = 0.1$, $\omega_c = 10$, $\beta = 0.5$. (**b**) $\Gamma(\tau)$ versus τ for the initial state specified by the Bloch vector $(1/\sqrt{3}, 1/\sqrt{3}, 1/\sqrt{3})$. The blue dashed curve shows the decay rate if the initial state is repeatedly measured; the solid red curve shows the decay rate if the optimal projective measurement is repeatedly made. Same parameters used as those used in (**a**). For $\tau = 1$ and $N = 3$, the difference in the survival probabilities is already 0.15. The inset shows the behavior of the survival probability as a function of the measurement interval with (solid, black curve) and without (dashed, purple curve) optimal measurements.
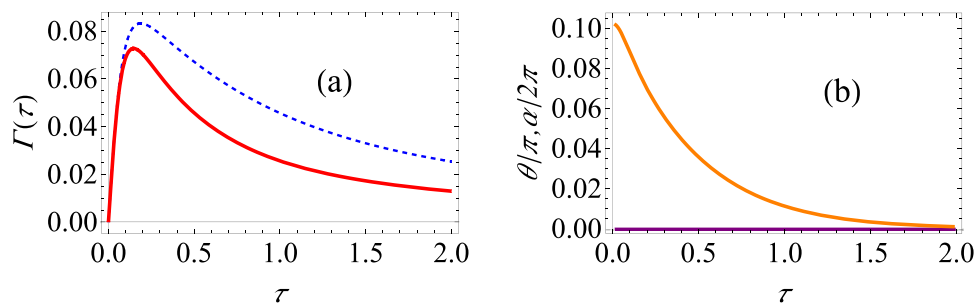

Figure 3. Graphs of the effective decay rate and the optimal spherical polar angles under making optimal projective measurements in the pure dephasing model. (**a**) $\Gamma(\tau)$ versus τ for the initial state specified by the Bloch vector $(1/\sqrt{10}, 0, \sqrt{9/10})$. The parameters used are the same as Fig. 2. (**b**) Graphs of the optimal spherical angles that maximize the survival probability. The orange curve traces the changes in θ/π (the normalized polar angle), while the purple curve traces the changes in $\alpha/2\pi$ (the normalized azimuthal angle which remains zero at all times).

be parallel to the Bloch vector of the density matrix at time τ. Hence in this case, the optimal projector to measure is $|\psi\rangle\langle\psi|$, corresponding to the initial state. The computational example shown inFig. 2(a) illustrates our predictions.

It should be emphasized, however, that if we make some other choice of the initial state that we repeatedly prepare, our optimized strategy does give us an advantage. We simply look for the case where the evolved Bloch vector (after removal of the evolution due to the system Hamiltonian) no longer remains parallel with the initial Bloch vector. Upon inspecting Eq. (9), we find that our optimized strategy can be advantageous if $n_z(0) \neq 0$ (excluding, of course, the cases $n_z(0) = \pm 1$). In other words, if the Bloch vector of the initial state does not lie in the equatorial plane, then the Bloch vector of this state at some later time will not remain parallel to the initial Bloch vector. In this case then, our optimal measurement scheme will give a higher survival probability as compared to repeatedly measuring the same initial state. This is illustrated in Fig. 2(b) where we show the effective decay rate and the survival probability after a single measurement for the initial state specified by the Bloch vector $(1/\sqrt{3}, 1/\sqrt{3}, 1/\sqrt{3})$. After the time at which the transition between the Zeno and the anti-Zeno regimes occurs, we clearly observe that the decay rate is lower when one makes the optimal projective measurements. Although this difference on first sight may appear insignificant, if we perform a relatively large number of repeated measurements, the difference can be very significant. For example, even for three measurements with measurement interval $\tau = 1$, we find that the quantum state has 0.15 greater survival probability with the optimized measurements as compared with the usual unoptimized strategy of repeatedly preparing the quantum state.

Another computational example has been provided in Fig. 3 where the initial state is now given by the Bloch vector $(1/\sqrt{10}, 0, \sqrt{9/10})$. In Fig. 3(a) we have again illustrated that our optimized strategy of repeatedly preparing the quantum state is better at protecting the quantum state as compared to the usual strategy. In Fig. 3(b) we have shown how the optimal projective measurement that needs to be performed changes with the measurement interval τ. In order to do so, we have parametrized the Bloch vector corresponding to $|\chi\rangle\langle\chi|$ using the usual spher-
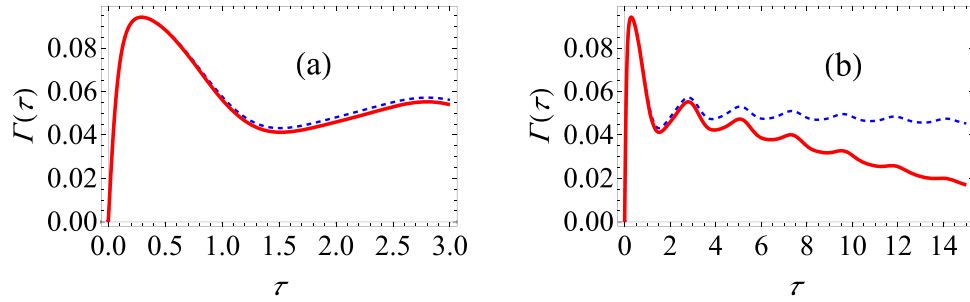
Figure 4. Graphs of the effective decay rate under making optimal projective measurements in the spin-boson model. (**a**) $\Gamma(\tau)$ versus τ (low temperature) for the state specified by $\theta = \pi/2$ and $\alpha = 0$. The blue dashed curve shows the decay rate in the spin boson model ($\Delta = 2$, $\varepsilon = 2$) if the initial state is repeatedly measured, and the solid red curve shows the effective decay rate with the optimal measurements. We have used $G = 0.01$, $\omega_c = 10$ and $s = 1$. (**b**) Same as (**a**) except that larger measurement intervals are also considered.

ical polar angles θ and α. Note that the value of the azimuthal angle α is expected to remain constant since we have $\alpha(\tau) = \arctan[n_y(\tau)/n_x(\tau)] = \alpha(0)$. On the other hand, the optimal value of the polar angle θ changes with the measurement interval. This is also expected since as the system dephases, $e^{-\gamma(\tau)} \to 0$, ensuring that $n_x(\tau)$, $n_y(\tau) \to 0$. Thus, for long measurement intervals, the system Bloch vector becomes effectively parallel to the z-axis. It follows that $\theta \to 0$ for long measurement intervals. These predictions are borne out by the behaviour of θ and α in Fig. 3(b).

Before moving on, let us discuss briefly how the measured described by the projector $|\chi\rangle\langle\chi|$ can be performed experimentally. After all, the state $|\chi\rangle$ can be any single-qubit state depending on the system-environment parameters, and experimentally the quantum state can be projected onto at most a few states. Let us suppose that one of these states is the state $|e\rangle$. To perform the projective measurement, we first find a unitary operator U_R such that $U_R|\chi\rangle = |e\rangle$. Then, instead of projecting onto $|\chi\rangle$, we can first perform the unitary operation U_R, and then project onto the state $|\chi\rangle$. We get the same survival probability. Since U_R is a single-qubit operation, it is experimentally accessible on a short time-scale[45,46]. In the Supplementary Material, we consider this measurement scheme with some errors included.

The Spin-Boson Model. We now consider the more general system-environment model given by the Hamiltonian

$$H = \frac{\varepsilon}{2}\sigma_z + \frac{\Delta}{2}\sigma_x + \sum_k \omega_k b_k^\dagger b_k + \sigma_z \sum_k (g_k^* b_k + g_k b_k^\dagger),$$

(12)

where Δ can be understood as the tunneling amplitude for the system, and the rest of the parameters are defined as before. This is the well-known spin-boson model[44,48,49], which can be considered as an extension of the previous two cases in that we now generally have both population decay and dephasing taking place. Experimentally, such a model can be realized, for instance, using superconducting qubits[37,50,51] and the properties of the environment can be appropriately tuned as well[52]. Once again, assuming that the system and the environment are interacting weakly with each other, we can use the master equation that we have used before [see Eq. (7)] to find the system density matrix as a function of time. However, we now have $H_S = \frac{\varepsilon}{2}\sigma_z + \frac{\Delta}{2}\sigma_x$ and $F = \sigma_z$.

Let us first choose as the initial state $n_x(0) = 1$ (or, in the words, the state that is paramterized by $\theta = \pi/2$ and $\alpha = 0$ on the Bloch sphere). In Fig. 4, we plot the behaviour of the effective decay rate as a function of the measurement interval using both our optimized strategy (the solid red lines) and the unoptimized usual strategy (the dotted, blue curves). It is clear from Fig. 4(a) that for relatively short measurement intervals, there is little to be gained by using the optimal strategy. As we have seen before in the pure dephasing case, for the state in the equatorial plane of the Bloch sphere, there is no advantage to be gained by following the optimized strategy. On the other hand, for longer time intervals τ, population decay can be considered to become more significant. Consequently, we see significant difference at long measurement intervals if we use the optimized strategy since it is only for longer measurement intervals that the state evolves significantly. This is precisely what we observe in Fig. 4(b). It is clear that our optimized signature displays a clearer signature of anti-Zeno behavior as compared with the unoptimized strategy at long measurement intervals.

Let us now also investigate how the the effective decay rate depends on the functional form of the spectral density. In Fig. 5(a,b), we investigate what happens in the case of a sub-Ohmic and a super-Ohmic environment respectively. The case of a sub-Ohmic environment with $s = 0.8$ is similar to the case with $s = 1$ (Ohmic environment) - once again, the optimal projective measurements decrease the decay rate substantially only at long measurement intervals. For the case of a super-Ohmic environment with $s = 2$ [see Fig. 5(b)], we find that the optimal projective measurements do not substantially lower the decay rate, even for long times. Thus, it is clear that the Ohmicity of the environment plays an important role in determining the usefulness of using the optimal projective measurements.

We now revert to the Ohmic environment case to present more computational examples. First, if $\varepsilon > \Delta$, then the effect of dephasing is expected to be more dominant than the effect of population decay. Results for this case are illustrated in Fig. 5(c). We see that there is negligible difference upon using the optimal measurements.
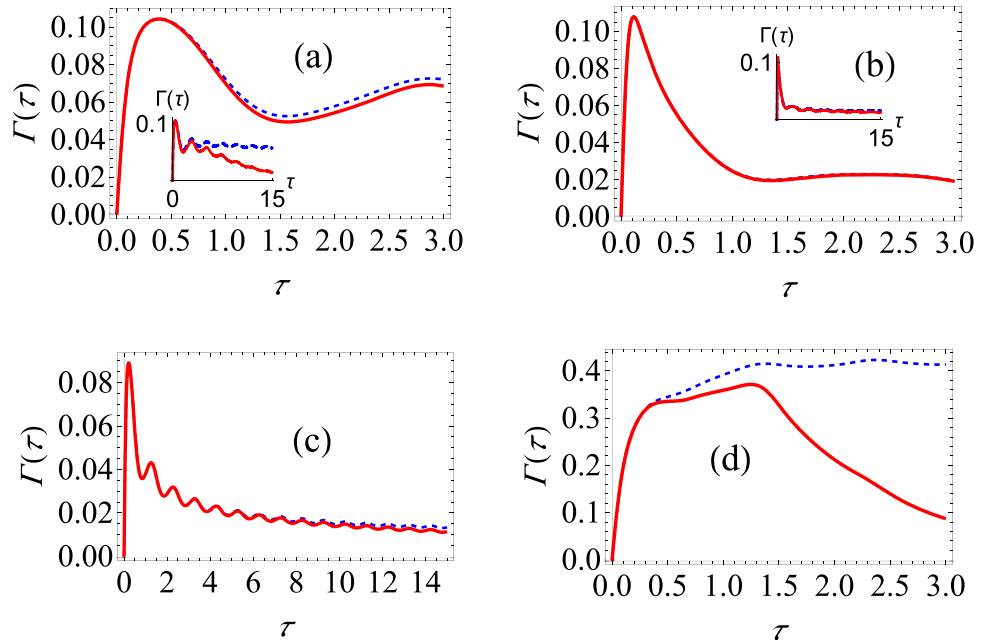
Figure 5. Graphs of the effective decay rate under making optimal projective measurements in the spin-boson model. (**a**) $\Gamma(\tau)$ versus τ (low temperature) for the state specified by $\theta = \pi/2$ and $\alpha = 0$. We have used the same parameters as in Fig. 4 except that we have now modeled a sub-Ohmic environment with $s = 0.8$. (**b**) Same as (**a**), except that we have now modeled a super-Ohmic environment with $s = 2.0$. (**c**) We have used $\varepsilon = 6$, $\Delta = 2$, while the rest of the parameters are $G = 0.025$, $\omega_c = 10$ and $s = 1$. (**d**) Same as (**c**), except that we now have $\varepsilon = 2$, $\Delta = 6$.

This agrees with what we found when we analyzed the pure dephasing model. We also analyze the opposite case where the effect of population decay is more dominant than the effect of dephasing. We now observe differences between the unoptimized and optimized decay rates for relatively short times [see Fig. 5(d)], and the difference becomes even bigger at longer times. In fact, while we observe predominantly only the Zeno effect with the unoptimized measurements, we observe very distinctly both the Zeno and the anti-Zeno regimes with the optimized measurements.

Large Spin System.   We now extend our study to a collection of two-level systems interacting with a common environment. In this case, the system-environment Hamiltonian is given by

$$H = \varepsilon J_z + \Delta J_x + \sum_k \omega_k b_k^\dagger b_k + 2J_z\sum_k (g_k^* b_k + g_k b_k^\dagger),$$

(13)

where J_x and J_z are the usual angular momentum operators and the environment is again modeled as a collection of harmonic oscillators. This Hamiltonian can be considered to be a generalization of the usual spin-boson model to a large spin $j = N_s/2$[28,53,54], where N_s is the number of two-level systems coupled to the environment. Physical realizations include a two-component Bose-Einstein condensate[55,56] that interacts with a thermal reservoir via collisions[54]. We first look at the pure dephasing case by settting $\Delta = 0$. In this case, the system dynamics can be found exactly. The system density matrix, in the eigenbasis of J_z, after removal of the evolution due to the system Hamiltonian can be written as $[\rho(t)]_{mn} = [\rho(0)]_{mn} e^{-i\Delta(t)(m^2-n^2)} e^{-\gamma(t)(m-n)^2}$. Here $\gamma(t)$ has been defined before, and $\Delta(t) = \sum_k 4|g_k|^2 \frac{[\sin(\omega_k t) - \omega_k t]}{\omega_k^2}$[28] describes the indirect interaction between the two-level systems due to their interaction with a common environment. For vanishingly small time t, $\Delta(t) \approx 0$. On the other hand, as t increases, the effect of $\Delta(t)$ becomes more pronounced. Thus, we expect significant differences as compared to the single two-level system case for long measurement intervals. However, it is important to note that we can no longer find the optimal measurements using the formalism presented before since our system is no longer a single two-level system. In principle, we need then need to carry out a numerical optimization procedure in order to find the projector $|\chi\rangle\langle\chi|$ such that the survival probability is maximized. Rather than looking at all possible states $|\chi\rangle$, we instead restrict ourselves to the SU(2) coherent states since these projective measurements are more readily experimentally accessible. In other words, we look at $|\chi\rangle\langle\chi|$ where

$$|\chi\rangle = |\zeta, J\rangle = (1 + |\zeta|^2)^{-J} \sum_{m=-J}^{m=J} \sqrt{\binom{2J}{J+m}} \zeta^{J+m}|J, m\rangle,$$

(14)

and $\zeta = e^{i\phi'}\tan(\theta'/2)$ with the states $|J, m\rangle$ being the angular momentum eigenstates of J_z. Suppose that we prepare the coherent state $|\eta, J\rangle$ with a fixed, pre-determined value of $\eta = e^{i\phi}\tan(\theta/2)$ repeatedly. In order to do so, we
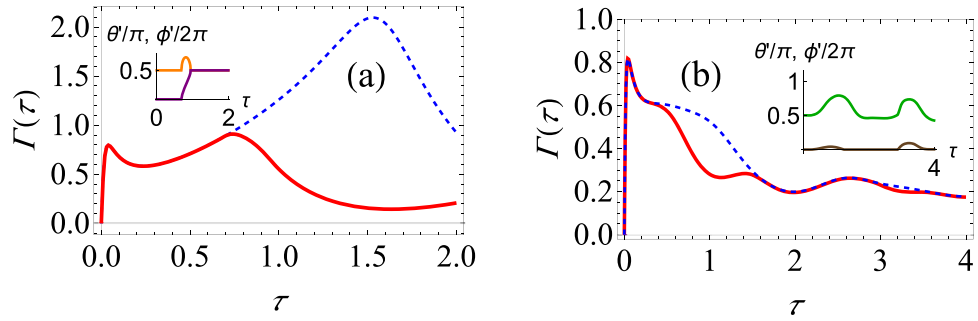
Figure 6. Graphs of the effective decay rate and the optimal spherical angles under making optimal projective measurements in the large spin model. (**a**) $\Gamma(\tau)$ versus τ for $J = 1$. Here we have $\Delta = 0$ (pure dephasing). The blue dashed curve shows the decay rate if the initial state is repeatedly measured; the red curve shows the decay rate if the optimal projective measurement is repeatedly made. The inset shows how the optimal measurements change with the measurement interval τ. The orange curve traces the change in θ'/π, while the purple curve traces the changes in $\phi'/2\pi$. We have used $G = 0.01$, $\omega_c = 50$, $\beta = 1$ and we take $\theta = \pi/2$ and $\phi = 0$ as parameters for the initial state. (**b**) Same as (**a**), except now that $\Delta = 2$, $\varepsilon = 2$, $\omega_c = 25$ and $\beta \to \infty$. The green curve traces the change in θ'/π, while the brown curve traces the change in $\phi'/2\pi$.

project, with time interval τ, the system state onto the coherent state $|\chi\rangle = |\zeta, J\rangle$. After each measurement, we apply a suitable unitary operator to arrive back at the state $|\eta, J\rangle$. Assuming the system-environment correlations are negligible, we find that

$$
\Gamma(\tau) = -\frac{1}{\tau} \ln \left\{ \left[\frac{|\zeta|}{1 + |\zeta|^2} \right]^{2J} \left[\frac{|\eta|}{1 + |\eta|^2} \right]^{2J} \sum_{m,n=-J}^{J} (\zeta^*\eta)^m (\eta^*\omega)^n \right.
$$
$$
\left. \times \binom{2J}{J+m} \binom{2J}{J+n} e^{-i\Delta(\tau)(m^2-n^2)} e^{-\gamma(\tau)(m-n)^2} \right\}.
$$
(15)

For equally spaced measurement time intervals, we numerically optimize Eq. (15) over the variables ϕ' and θ'. We present a computational example in Fig. 6(a). We take as the initial state the SU(2) coherent state with $\theta = \pi/2$ and $\phi = 0$ and we let $J = 1$. This is simply the generalization of the pure dephasing model that we have looked at before to $J = 1$. Previously, there was no difference in the optimized and unoptimized probabilities. Now, we see that because of the indirect interaction, there is a very noticeable difference. Where we observe the Zeno regime with the unoptimized measurements, we instead see the anti-Zeno regime with the optimized measurements. Furthermore, the survival probability can be significantly enhanced using the optimized measurements.

For completeness, we have also considered the more general case with $\Delta \neq 0$. In this case, the system dynamics cannot be solved exactly, so we resort again to the master equation to find the system dynamics. With the system dynamics known, we again find the projector, parametrized by θ' and ϕ', such that the decay rate is minimized. Results are illustrated in Fig. 6(b). Once again, using optimizing projective measurements changes the Zeno and anti-Zeno behaviour.

Discussion

Our central idea is that instead of repeatedly preparing the quantum state of a system using only projective measurements, we can repeatedly prepare the quantum state by using a combination of both projective measurements and unitary operations. This then allows us to consider the projective measurements that yield the largest survival probability. For the case of the central quantum system being a simple two-level system, we have derived an expression that optimizes the survival probability, or equivalently the effective decay rate. This expression implies that the optimal projective measurement at time τ corresponds to the projector that is parallel to the Bloch vector of the system's density matrix at that time. We consequently applied our expression for the optimized survival probability to various models. For the population decay model, we found that beyond a critical time τ^*, we should flip the measurement and start measuring the ground state rather than the excited state. For the pure dephasing model, we found that for states prepared in the equatorial plane of the Bloch sphere, it is optimal to measure the initial state - determining and making the optimal projective measurement has no effect on the effective decay rate. In contrast, for states prepared outside of the equatorial plane, the effect of making the optimal projective measurement substantially lowers the effective decay rate in the anti-Zeno regime. In the general spin-boson model, we have found that there can be a considerable difference between the optimized and unoptimized effective decay rates, which translates to a difference in the Zeno and anti-Zeno behavior. We then extended our analysis to the case of large spin systems. We found that the indirect interaction between the two-level systems causes the optimal measurements to be even more advantageous. One possible objection to our results is that our scheme to minimize the effective decay rate seems to rely very much on knowing the system-environment parameters (and hence the detailed system evolution) precisely. In the Supplementary Material, we show that this is not the case, and our scheme is quite robust against errors in the system-environment parameters. The results of this paper show that by exploiting the choice of the measurement to be performed on the system, we could more

effectively 'freeze' the state of the quantum system. Experimental implementations of the ideas presented in this paper are expected to be important for measurement-based quantum control.

References

1. Misra, B. & Sudarshan, E. C. G. The zeno's paradox in quantum theory. *J. Math. Phys. (NY)* **18**, 756 (1977).
2. Kofman, A. G. & Kurizki, G. Acceleration of quantum decay processes by frequent observations. *Nature (London)* **405**, 546 (2000).
3. Koshino, K. & Shimizu, A. Quantum zeno effect by general measurements. *Phys. Rep.* **412**, 191 (2005).
4. Facchi, P., Gorini, V., Marmo, G., Pascazio, S. & Sudarshan, E. Quantum zeno dynamics. *Phys. Lett. A* **275**, 12 (2000).
5. Fischer, M. C., Gutiérrez-Medina, B. & Raizen, M. G. Observation of the quantum zeno and anti-zeno effects in an unstable system. *Phys. Rev. Lett.* **87**, 040402 (2001).
6. Facchi, P. & Pascazio, S. Quantum zeno subspaces. *Phys. Rev. Lett.* **89**, 080401 (2002).
7. Barone, A., Kurizki, G. & Kofman, A. G. Dynamical control of macroscopic quantum tunneling. *Phys. Rev. Lett.* **92**, 200403 (2004).
8. Maniscalco, S., Piilo, J. & Suominen, K.-A. Zeno and anti-zeno effects for quantum brownian motion. *Phys. Rev. Lett.* **97**, 130402 (2006).
9. Segal, D. & Reichman, D. R. Zeno and anti-zeno effects in spin-bath models. *Phys. Rev. A* **76**, 012109 (2007).
10. Facchi, P. & Pascazio, S. Quantum zeno dynamics: mathematical and physical aspects. *J. Phys. A: Math. Theor.* **41**, 493001 (2008).
11. Wang, X.-B., You, J. Q. & Nori, F. Quantum entanglement via two-qubit quantum zeno dynamics. *Phys. Rev. A* **77**, 062339 (2008).
12. Maniscalco, S., Francica, F., Zaffino, R. L., Lo Gullo, N. & Plastina, F. Protecting entanglement via the quantum zeno effect. *Phys. Rev. Lett.* **100**, 090503 (2008).
13. Zheng, H., Zhu, S. Y. & Zubairy, M. S. Quantum zeno and anti-zeno effects: Without the rotating-wave approximation. *Phys. Rev. Lett.* **101**, 200404 (2008).
14. Ai, Q., Li, Y., Zheng, H. & Sun, C. P. Quantum anti-zeno effect without rotating wave approximation. *Phys. Rev. A* **81**, 042116 (2010).
15. Facchi, P. & Ligabò, M. Quantum zeno effect and dynamics. *J. Phys. A: Math. Theor.* **51**, 022103 (2010).
16. Chen, P.-W., Tsai, D.-B. & Bennett, P. Quantum zeno and anti-zeno effect of a nanomechanical resonator measured by a point contact. *Phys. Rev. B* **81**, 115307 (2010).
17. Fujii, K. & Yamamoto, K. Anti-zeno effect for quantum transport in disordered systems. *Phys. Rev. A* **82**, 042109 (2010).
18. Thilagam, A. Zeno–anti-zeno crossover dynamics in a spin–boson system. *J. Phys. A: Math. Theor.* **43**, 155301 (2010).
19. Militello, B., Scala, M. & Messina, A. Quantum zeno subspaces induced by temperature. *Phys. Rev. A* **84**, 022106 (2011).
20. Xu, D. Z., Ai, Q. & Sun, C. P. Dispersive-coupling-based quantum zeno effect in a cavity-qed system. *Phys. Rev. A* **83**, 022107 (2011).
21. Zhang, Z.-T. & Xue, Z.-Y. Demonstration of quantum zeno effect in a superconducting phase qubit. *JETP Letters* **93**, 349–353 (2011).
22. Cao, X., Ai, Q., Sun, C.-P. & Nori, F. The transition from quantum zeno to anti-zeno effects for a qubit in a cavity by varying the cavity frequency. *Phys. Lett. A* **376**, 349–357 (2012).
23. Raimond, J. M. *et al.* Quantum zeno dynamics of a field in a cavity. *Phys. Rev. A* **86**, 032120 (2012).
24. Smerzi, A. Zeno dynamics, indistinguishability of state, and entanglement. *Phys. Rev. Lett.* **109**, 150410 (2012).
25. Wang, S.-C., Li, Y., Wang, X.-B. & Kwek, L. C. Operator quantum zeno effect: Protecting quantum information with noisy two-qubit interactions. *Phys. Rev. Lett.* **110**, 100505 (2013).
26. McCusker, K. T., Huang, Y.-P., Kowligy, A. S. & Kumar, P. Experimental demonstration of interaction-free all-optical switching via the quantum zeno effect. *Phys. Rev. Lett.* **110**, 240403 (2013).
27. Thilagam, A. Non-markovianity during the quantum zeno effect. *J. Chem. Phys.* **138**, 175102 (2013).
28. Chaudhry, A. Z. & Gong, J. Zeno and anti-zeno effects on dephasing. *Phys. Rev. A* **90**, 012101 (2014).
29. Stannigel, K. *et al.* Constrained dynamics via the zeno effect in quantum simulation: Implementing non-abelian lattice gauge theories with cold atoms. *Phys. Rev. Lett.* **112**, 120406 (2014).
30. Zhu, B. *et al.* Suppressing the loss of ultracold molecules via the continuous quantum zeno effect. *Phys. Rev. Lett.* **112**, 070404 (2014).
31. Schäffer, F. *et al.* Experimental realization of quantum zeno dynamics. *Nat. Commun.* **5**, 3194 (2014).
32. Signoles, A. *et al.* Confined quantum Zeno dynamics of a watched atomic arrow. *Nat. Phys.* **10**, 715–719 (2014).
33. Debierre, V., Goessens, I., Brainis, E. & Durt, T. Fermi's golden rule beyond the zeno regime. *Phys. Rev. A* **92**, 023825 (2015).
34. Kiilerich, A. H. & Mølmer, K. Quantum zeno effect in parameter estimation. *Phys. Rev. A* **92**, 032124 (2015).
35. Qiu, J. *et al.* Quantum zeno and zeno-like effects in nitrogen vacancy centers. *Sci. Rep.* **5**, 17615 (2015).
36. Zhang, Y.-R. & Fan, H. Zeno dynamics in quantum open systems. *Sci. Rep.* **5**, 11509 (2015).
37. Slichter, D. H. *et al.* Quantum zeno effect in the strong measurement regime of circuit quantum electrodynamics. *New. J. Phys.* **18**, 053031 (2016).
38. Chaudhry, A. Z. A general framework for the quantum zeno and anti-zeno effects. *Sci. Rep.* **6**, 29497 (2016).
39. Mueller, M. M., Gherardini, S. & Caruso, F. Stochastic quantum Zeno-based detection of noise correlations. *Sci. Rep.* **6**, 38650 (2016).
40. Gherardini, S., Gupta, S., Cataliotti, F. S., Smerzi, A., Caruso, F. & Ruffo, S. Stochastic quantum Zeno by large deviation theory. *New J. Phys.* **18**, 013048 (2016).
41. Chaudhry, A. Z. The quantum Zeno and anti-Zeno effects with strong system-environment coupling. e-print arXiv:1701.07283 (2017).
42. Matsuzaki, Y., Saito, S., Kakuyanagi, K. & Semba, K. Quantum zeno effect with a superconducting qubit. *Phys. Rev. B* **82**, 180518 (2010).
43. Scully, M. O. & Zubairy, M. S. *Quantum optics* (Cambridge University Press, Cambridge, 1997).
44. Breuer, H.-P. & Petruccione, F. *The Theory of Open Quantum Systems* (Oxford University Press, Oxford, 2007).
45. Berezovsky, J., Mikkelsen, M. H., Stoltz, N. G., Coldren, L. A. & Awschalom, D. D. Picosecond Coherent Optical Manipulation of a Single Electron Spin in a Quantum Dot. *Science* **320**, 349 (2008).
46. Lucero, E. *et al.* High-Fidelity Gates in a Single Josephson Qubit. *Phys. Rev. Lett.* **100**, 247001 (2008).
47. Risté, D., van Leeuwen, J. G., Ku, H.-S., Lehnert, K. W. & DiCarlo, L. Initialization by Measurement of a Superconducting Quantum Bit Circuit. *Phys. Rev. Lett.* **109**, 050507 (2012).
48. Leggett, A. J. *et al.* Dynamics of the dissipative two-state system. *Rev. Mod. Phys.* **59**, 1–85 (1987).
49. Weiss, U. *Quantum dissipative systems* (World Scientific, Singapore, 2008).
50. Clarke, J. & Wilhelm, F. Superconducting quantum bits. *Nature* (*London*) **453**, 1031 (2008).
51. You, J. & Nori, F. Atomic physics and quantum optics using superconducting circuits. *Nature* (*London*) **474**, 589 (2011).
52. Le Hur, K. Kondo resonance of a microwave photon. *Phys. Rev. B* **85**, 140506 (2012).
53. Vorrath, T. & Brandes, T. Dynamics of a large spin with strong dissipation. *Phys. Rev. Lett.* **95**, 070402 (2005).
54. Bar-Gill, N., Rao, D. D. B. & Kurizki, G. Creating nonclassical states of bose-einstein condensates by dephasing collisions. *Phys. Rev. Lett.* **107**, 010404 (2011).
55. Gross, C., Zibold, T., Nicklas, E., Estève, J. & Oberthaler, M. K. Nonlinear atom interferometer surpasses classical precision limit. *Nature* **464**, 1165–1169 (2010).
56. Riedel, M. F. *et al.* Atom-chip-based generation of entanglement for quantum metrology. *Nature* **464**, 1170–1173 (2010).

Acknowledgements

Author Contributions

A.Z.C. came up with idea for this work. M.J.A. carried out the calculations and numerical simulations. Both A.Z.C. and M.J.A. contributed towards the writing of the manuscript.

Additional Information

Supplementary information accompanies this paper at doi:10.1038/s41598-017-11787-9.

Competing Interests: The authors declare that they have no competing interests.

Publisher's note: Springer Nature remains neutral with regard to jurisdictional claims in published maps and institutional affiliations.